RSC Advances

PAPER

View Article Online
View Journal | View Issue

Cite this: *RSC Adv.*, 2025, **15**, 34049

Structure–property relationship and design of carbazole naphthalene-based linear materials for organic and perovskite photovoltaics

Aqsa Ghaffar,[a] Zobia Irshad,[*b] Riaz Hussain,[*a] Ayesha Ghaffar,[a] Hany W. Darwish,[c] Malik Muhammad Asif Iqbal[a] and Muhammad Adnan[*b]

To enhance the stability and efficiency of organic and perovskite solar cells, hole transport materials (HTMs) have garnered significant research attention. In this study, eight novel donor-based HTMs with a D–C–D–B–A (donor–core–donor–bridge–acceptor) architecture are designed by substituting the electronegative oxygen atom in the synthetic reference molecule **AQ-R** with various electron-withdrawing groups. This structural modification aimed to expand and fine-tune the photovoltaic and optoelectronic properties of organic and perovskite solar cells. Comprehensive computational analyses are conducted using density functional theory (DFT) and time-dependent (TD-DFT) approaches. The objective of all these analyses is to investigate the molecular geometries, optical properties, and photovoltaic performance. Key parameters that are determined include the molar absorption coefficient, frontier molecular orbitals, density of states, transition density matrix, electron density difference, light harvesting efficiency, excitation and binding energies, reorganization energies, and charge transfer characteristics. Furthermore, device-relevant properties such as open-circuit voltage, fill factor, and power conversion efficiency are estimated for the synthetic reference **AQ-R** and all designed materials (**AQ-1–AQ-8**). The newly developed HTMs (**AQ-1** to **AQ-8**) showed lower excitation and binding energies, indicating their strong potential for efficient charge transport. Overall, this work highlights end-capped structural tuning as a promising strategy for optimizing donor materials, offering a viable pathway to boost the performance of organic and perovskite photovoltaics.

Received 18th August 2025
Accepted 1st September 2025

DOI: 10.1039/d5ra06095h

rsc.li/rsc-advances

1 Introduction

One of the topics that people discuss the most around the globe these days is the energy crisis.[1] This has resulted from an over-dependence on non-renewable energy sources, which will ultimately run out and release greenhouse gases into the atmosphere, causing a calamity for the ecosystem.[2] To address this issue, a variety of options have been investigated, including biomass, organic, and perovskite solar cells, and wind energy.[3] The most capable of these are photovoltaic resources, which can convert solar energy into electrical power and are also a source of workable and sustainable ways to fulfill the increasing energy demands of the world.[4–6] Solar parks and residential rooftop installations have drawn significant attention, especially in the world's sunnier regions. Sunshine is transformed into electrical power by organic and perovskite solar cells using a process known as the photoelectric effect.[7] The world has been enthralled with organic and perovskite solar cells due to their comparatively reduced production costs, versatility, good power conversion efficiency, lightweight nature, and adjustable energy levels.[8]

Perovskite solar cells (PSCs) have a maximum power conversion efficiency (PCE). They have consistently displayed a pattern of constant breakthroughs and advancement.[9–13] Now, the certified PCE is more than 27%.[14] High-efficiency PSCs are primarily made up of an electrode on both sides, a light absorption layer, and a charge transference layer. It is possible to achieve the desired energy gap and excellent hole abstraction capability, along with a perovskite shield for the hole transport layer, by modifying the compound assembly of hole transport materials (HTMs)[15–21] or by using additive regulation techniques.[22,23] To design and create a reference molecule (H580), the carbazole linking unit on the molecular structure was expanded; in short, naphthalene was used to replace the benzene on the carbazole ring. According to the results, H580 had a higher glass transition temperature, improved hydrophobicity, higher carrier mobility, and a deeper HOMO level.[24] H580 was then used as the interfacial material between

[a]*Department of Chemistry, University of Okara, 56300, Pakistan. E-mail: riazhussain@uo.edu.pk*

[b]*Graduate School of Energy Science and Technology, Chungnam National University, Daejeon, 34134, Republic of Korea. E-mail: chem.zobia@gmail.com; adnan5750@gmail.com; adnan@cnu.ac.kr*

[c]*Department of Pharmaceutical Chemistry, College of Pharmacy, King Saud University, P.O. Box 2457, Riyadh 11451, Saudi Arabia*

perovskite and spiro-OMeTAD due to the cyano group's greater passivating effect for the perovskite films. When H580 is used as an interfacial layer, the device's maximum PCE reaches 22.55%, and its stability is also markedly increased. Among many hole transport materials, poly[bis(4-phenyl)(2,4,6-trimethylphenyl) amine] (PTAA) is one of the most promising options because of its stability, conductivity, mechanical flexibility, transparency to visible light, and ease of production.[25]

The three types of HTMs are polymer, organic small-sized molecules, and inorganic substances. Various dopant-free hole-transporting materials (HTMs) used in perovskite solar cells (PSCs) are categorized into three types: inorganic, polymeric, and small-molecule HTMs. PSCs have undergone rapid progress, achieving power conversion efficiencies (PCEs) above 22%.[26] Due to their straightforward assembly, ease of management, and consistent molecular weight with excellent repeatability, organic minor molecule substances have garnered great interest.[27] Organic minor-size molecule substances can be broadly classified into linear-type,[28,29] spiro-type,[30,31] star-shaped,[32–34] and so on, based on the various molecular forms. Moreover, devices based on the new HTM showed good long-term stability and maintained over 80% of their initial efficiency.[35] All newly developed spirofused molecules are spirocore-based hole-transporting materials (HTMs) and are promising candidates for highly efficient and stable PSCs, paving the way for the future commercialization of PSCs. Notable benefits of the linear molecule structure are its reduced cost, easier synthesis, and more condensed assembly.[36] The carbazole linking component on the chemical assembly was expanded to create an organic molecule known as H580. In short, naphthalene was substituted for the benzene in the carbazole.

Recent strategies in hole-transport materials (HTMs) have expanded beyond linear architectures to include star-shaped, spiro-based, and polymeric frameworks—each presenting distinct trade-offs in charge mobility, morphological robustness, and scalability.[37,38] Star-shaped HTMs, such as DPAMes-TT and TPA-TT, exhibit enhanced π–π stacking, narrow band gaps, and favorable HOMO alignment, achieving high efficiencies (~19.3%) while minimizing aggregation and eliminating dopants.[38,39] Spiro-based systems, particularly spiro-OMeTAD, remain a benchmark due to their excellent film-forming properties and energy-level alignment; however, they suffer from high costs and a reliance on hygroscopic dopants that impair stability. Although polymeric HTMs provide mechanical resilience and scalable processing, they frequently suffer from repeatability and batch-to-batch inconsistencies. Due to interfacial and morphological complexity, computational descriptors such as HOMO level and reorganization energy help with initial screening but need to be verified through empirical device testing.

Here, we designed eight new ecologically acceptable donor molecules (**AQ-1** to **AQ-8**) that are of the D–C–D–B–A (donor–core–donor–bridge–acceptor) kind by substituting an electron-withdrawing group for the electronegative O in the reference molecule (**AQ-R**).[24] Following that, we implement a variety of quantum chemical techniques to optimize these created materials (**AQ-1** to **AQ-8**) to assess their competence for solar cell devices. The extraordinary optical and photovoltaic features of these materials (**AQ-1** to **AQ-8**) make them noteworthy.[40–45] Using quantum chemical techniques, we investigate various characteristics, including the FMO, the HOMO–LUMO narrow band distance, the density of states (DOS), the transition dipole moment (TDM), the recombination efficiency (RE), the reorganization energy of electrons and holes, the V_{oc}, and composite studies. This comprehensive theoretical analysis reveals important information regarding the unique hidden capacity of the designed (**AQ-1** to **AQ-8**) substances to generate efficient organic and PSC devices.[45]

2 Computational methodology

The quantum mechanical method was computed using the Gaussian 09 version of the program,[46] and the results were represented using the famous GaussView 5.0 version application.[47] The approach to be used in this theoretical study was determined by calculating the density functional theory (DFT) and optimizing the geometry of **AQ-R** using six alternative functionals at ground level: B3LYP,[48] CAMB3LYP,[49] M06,[50] M06-2X,[51] MPW1PW91 (ref. 52) and ωB97XD,[53] and a basis set 6-31G(d,p). (TD-DFT) computations were performed by employing the selected dichloromethane solvent for **AQ-R** in an excited state after its geometry was optimized. According to reports in the literature, in the case of **AQ-R**, dichloromethane was preferred as the solvent (medium) for the suggested materials.[24] This allowed for the creation of an environment that was comparable to the reference environment. The polarizable continuum model (PCM) is used to calculate the electrical and optical properties of compounds in the presence of dichloromethane solvent.[54] When we compared the observed absorption value of **AQ-R** to its UV-Vis absorption, we determined that the values obtained from MPW1PW91/631G(d,p) matched the experimental result. We subsequently used this DFT functional to carry out further characterization. As a result, the intended compounds (**AQ-1** to **AQ-8**) were solved at the theoretical level of MPW1PW91/631G(d,p). We can easily study the oscillator strength, open-circuit voltage (V_{oc}), excitation, and RE, LHE (light harvesting efficiency), and FMO (frontier molecular orbital) analysis for the **AQ-R** compound and the newly considered materials (**AQ-1** to **AQ-8**). The plots for absorption, the DOS analysis, and the TDM investigation were obtained using PyMOlyze 2.0,[55] Origin 6.0, and Multiwfn 3.7,[56] respectively. Furthermore, the RE data for the hole (λ_{hole}) and electron ($\lambda_{electron}$) were calculated using the Marcus rate equation.[57] The subsequent eqn (1) and (2) were used to carry out these RE estimates, where the energy at the neutral, cationic, and anion states, and also the excited and ground states, are represented by symbols E_0, E_+, E_-, E_0^+, E_0^-, and E_+^0, E_-^0 respectively.

$$\lambda_e = [E_0^- - E_-] + [E_-^0 - E_0] \quad (1)$$

$$\lambda_h = [E_0^+ - E_+] + [E_+^0 - E_0] \quad (2)$$

3 Results and discussion

We initially optimized the **AQ-R** molecule using a range of DFT functionals and selected the ideal DFT functional, which has UV values that are either closer to or comparable to the reported UV value of the standard material (**AQ-R**). Effective DFT functionals at 631G(d,p) in both vapor and solvent mediums, namely: B3LYP (439.16), CAMB3LYP (347.66), M06 (419.49), M06-2X (356.23), MPW1PW91 (418.51), and ωB97XD (341.24) have been employed for this optimization. Utilizing each of these DFT functionals, it was unexpectedly discovered that the **AQ-R** molecule displays a highly bathochromic shift and outstanding data of UV-visible spectrum, as revealed in Fig. 3 and recorded in Table S1 for B3LYP, CAMB3LYP, M06, M06-2X, MPW1PW91, and ωB97XD. Following this optimization, we selected the MPW1PW91-6-31G(d,p) functional for additional material characterization of the produced compounds **AQ-1** to **AQ-8** and **AQ-R**. The value attained with MPW1PW91-6-31G(d,p) is 418.51 nm, which is substantially closer and comparable to the UV-value of **AQ-R** obtained experimentally, which is 401 nm, as exposed in Fig. 1. Fig. S1 shows the optimum geometry of intended materials that we first optimized at the ground state after choosing the DFT functional, and recently generated chemical compounds with modified end-capped groups are shown in Fig. 2. Table S4 lists the dihedral angles for **AQ-R** and **AQ-1** to **AQ-8**. It was discovered that all the molecules (**AQ-R**, **AQ-1** to **AQ-8**) with optimized structures had similar geometries because of comparable dihedral angles.

3.1 Frontier molecular orbital

FMO is one of the key elements influencing a molecule's opto-electronic and chemical characteristics. The HOMO/LUMO charge distribution pattern of the **AQ-R** molecule and molecular design structures **AQ-1** to **AQ-8** are shown in Fig. 3 and were computed at the DFT/MPW1PW91 6-31G(d,p) state in DCM medium. Understanding the position of charge distribution in major conversion orbitals of photovoltaic cells is useful in determining the likelihood of charge transmission in a compound from donor to acceptor. The distribution of electronic density among the ground and excited energy levels is displayed by the FMOs analysis. The process of electron excitation involves the effective transport of negative charges from (H) to (L).

The transmission band FMOs, also known as LUMOs, are mostly located in the electron-accepting region of the compound, as compared the valence band FMOs, also known as HOMOs, are largely positioned in the electron-donating zone. The HOMO (H) energy levels of **AQ-R** and newly established molecules **AQ-1** to **AQ-8** were −4.78 eV, −5.02 eV, −5.02 eV, −5.02 eV, −5.02 eV, −5.01 eV, −4.95 eV, −5.01 eV, and −5.01 eV, respectively. On the other hand, −1.20 eV, −3.47 eV, −3.26 eV, −3.34 eV, −3.46 eV, −3.32 eV, −1.86 eV, −3.55 eV, and −3.30 eV are the LUMO energy states of recently considered compounds as shown in Fig. 3. The alteration in energy gaps amid these binary orbitals is known as the energy gap, which affects charge movement, light absorption, and organic and perovskite solar cells efficiency, determined using $E_g = E_L - E_H$. Charges can be shifted from the (H) level to the (L) state when the band gap is narrow. When (H) is large and (L) is small, the bandgap is

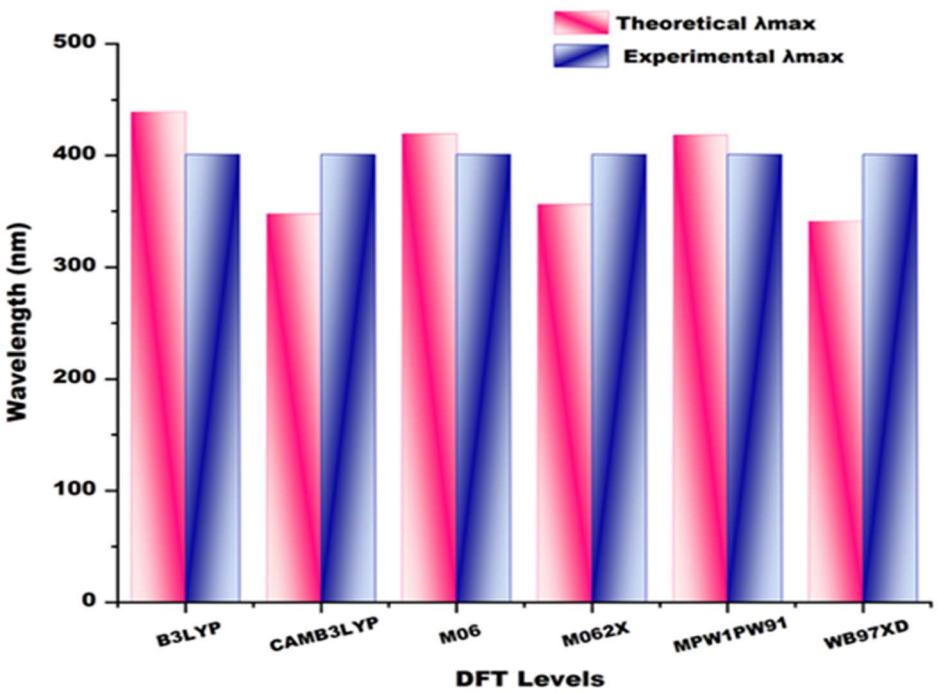

Fig. 1 Comparison of experimental and theoretically estimated absorption maxima (λ_{max}) of reference AQ-R at different DFT levels in solvent (DCM).

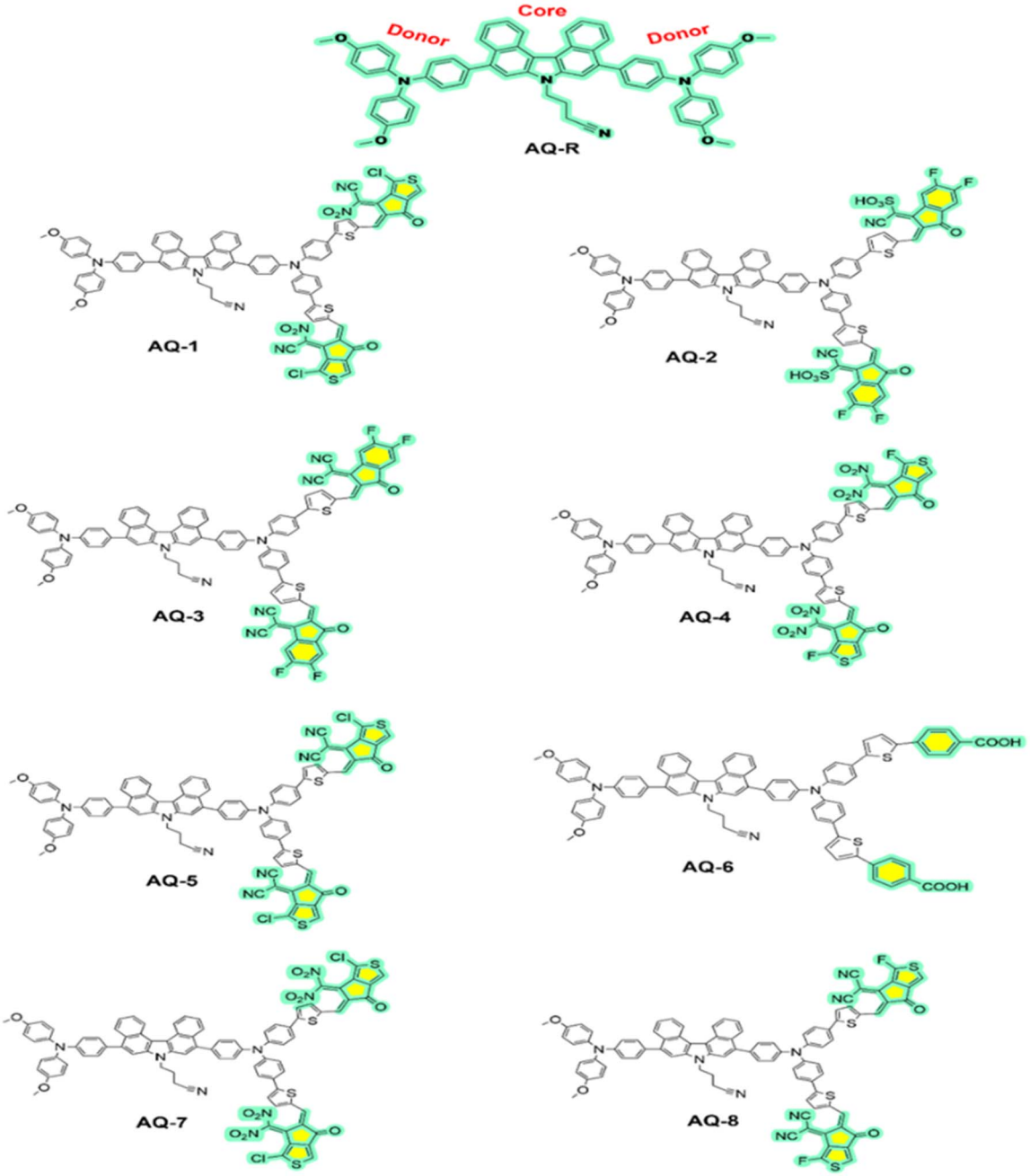

Fig. 2 Chemical structures of the synthetic reference molecule (AQ-R) and proposed (AQ-1–AQ-8) molecules.

decreased, aiding in the development of extremely efficient OSCs. The energy gap values are 3.58 eV, 1.55 eV, 1.77 eV, 1.68 eV, 1.56 eV, 1.70 eV, 3.09 eV, 1.46 eV, and 1.71 eV for **AQ-R** and the recently designed compounds (**AQ-1** to **AQ-8**) as listed in Table S2.

The energy difference in enhancing sequence is given as: **AQ-7** < **AQ-1** < **AQ-4** < **AQ-3** < **AQ-5** < **AQ-8** < **AQ-2** < **AQ-6** < **AQ-R**. In organic and perovskite solar cells, materials with a narrow bandgap are thought to be extremely efficient and desirable, and all of our developed molecules (**AQ-1** to **AQ-8**) have a smaller bandgap than the **AQ-R**. The **AQ-7** molecule is expected to exhibit better photovoltaic performance among all newly developed compounds due to its smaller bandgap and larger charge dispersion due to the strong electron-withdrawing moieties (NO_2 and Cl). The eight created molecules, **AQ-1** to **AQ-8**, have more uniformly dispersed charges among the donors, core, acceptors, and spacers as compared to **AQ-R**, according to an FMO study, which demonstrates our effective end-capped engineering on **AQ-R**'s terminals.

3.2 Optical properties

We determined the optical and photophysical features of **AQ-R** and recently developed (**AQ-1** to **AQ-8**) compounds, utilizing UV-

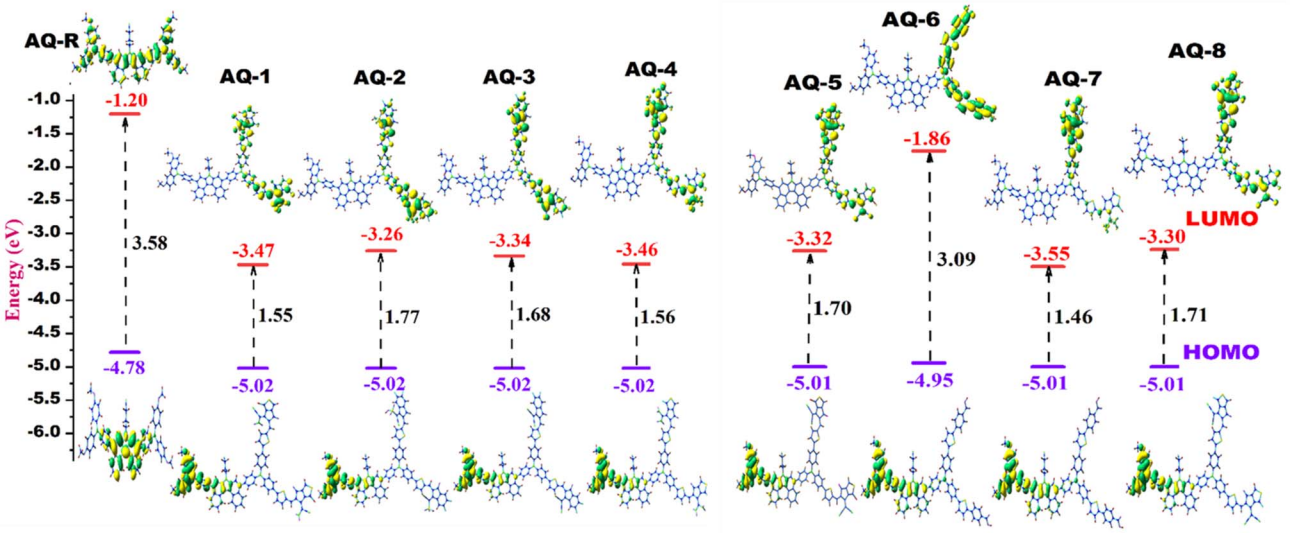

Fig. 3 Pictorial representation of HOMO and LUMO dispersion of the synthetic reference AQ-R and modelled AQ-1 to AQ-8 molecules.

Vis investigation at MPW1PW91/6-31G(d,p) DFT state in both gaseous phase and (DCM) solvent. Tables 2 and S3 demonstrate examples of novelty intended (**AQ-1** to **AQ-8**) compounds along with reportedly computed λ_{max} and oscillator frequency in solvent, besides the gaseous medium, respectively.

A major determinant of the maximum bathochromic value (λ_{max}) is conjugation, which is enhanced by modifying terminal moieties. The standard molecules' (λ_{max}) were calculated practically to be 401 nm, but DFT computations reveal that in the gaseous and (DCM) phases, they are, respectively, 408.76 and 418.51 nm. In (DCM), the specified molecules (**AQ-1** to **AQ-8**) displayed extreme absorbance. The developed (**AQ-1** to **AQ-8**) molecules have supreme solubility parameters of 751.15 nm, 674.12 nm, 687.58 nm, 745.32 nm, 694.36 nm, 430.78 nm, 799.12 nm, and 684.20 nm. When related to other manufactured and reference (**AQ-R**) compounds, the **AQ-7** molecule shows a bathochromic shift, with the highest λ_{max} value increasing with absorbance value. The proposed compounds (**AQ-1** to **AQ-8**) and reference **AQ-R** have the following gas phase absorption values: 612.84 nm, 635.33 nm, 582.82 nm, 608.18 nm, 436.40 nm, 424.65 nm, 638.07 nm, 431.73 nm, and 408.76 nm. Generally, shifting the λ_{max} towards the red end of the absorption band results in an increase in the PCE of a PSC. As shown in Fig. 4, the absorption band of **AQ-1** to **AQ-8** materials is red-shifted due to the exchange of a variety of terminal acceptor moieties in the **AQ-R** for a side-chain donor unit. Due to the nitro groups, **AQ-7** and **AQ-1** displayed the greatest electron-withdrawing effect and the lowest band gap among all the developed molecules. The results of this experiment showed that all eight compounds (**AQ-1** to **AQ-8**) had determined absorptions (λ_{max}) higher than the reference (**AQ-R**).

3.3 Quantum chemical indices

Thus, quantum mechanical reactivity parameters such as chemical potential (μ), softness (S), hardness (η), electrophilicity index (ω), electronegativity (χ), adiabatic and vertical

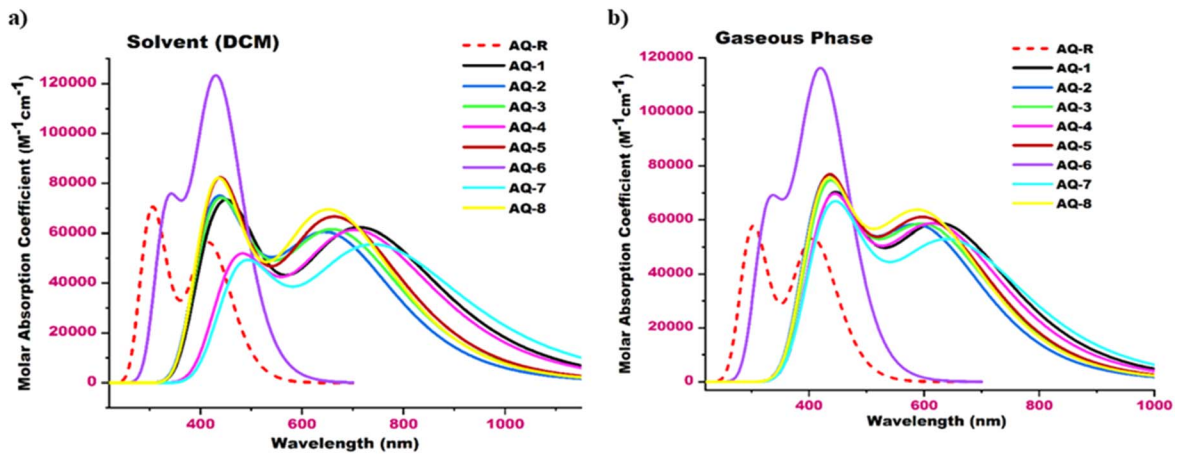

Fig. 4 Comparison of the UV-visible absorption spectrum of (AQ-R) with newly suggested structures (AQ-1 to AQ-8) in dichloromethane (a) and gaseous phase (b).

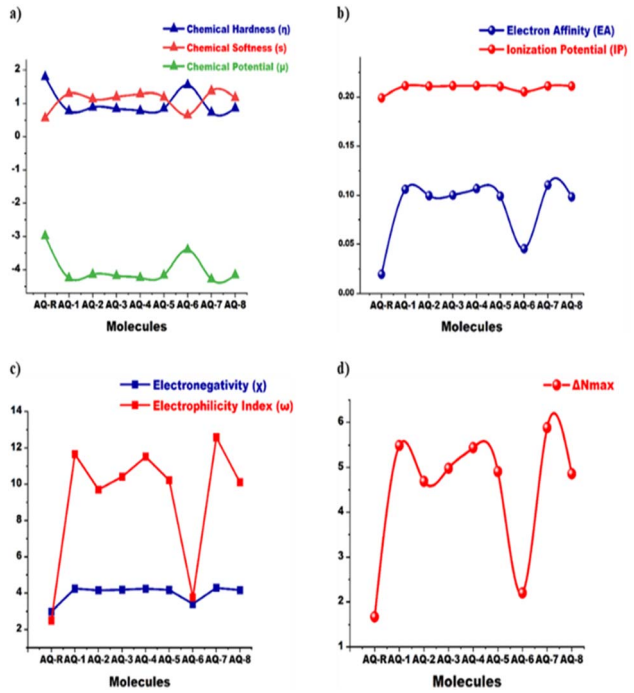

Fig. 5 Graphical illustration and comparison of various quantum chemical indices: (a) chemical potential, hardness, and softness, (b) IP and EA, (c) electronegativity and electrophilicity index, (d) charge transfer of synthetic reference **AQ-R** and newly designed **AQ-1** to **AQ-8** molecules.

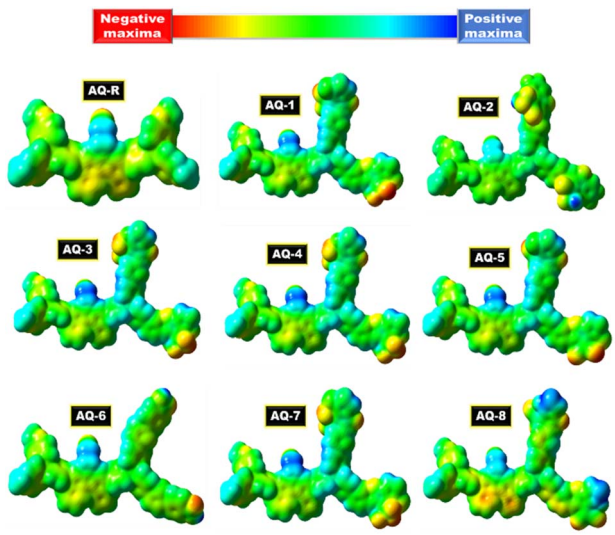

Fig. 6 Electrostatic potential analysis of synthetic reference **AQ-R** and the designed **AQ-1** to **AQ-8** molecules.

electron affinity (EA_a/EA_v), adiabatic and vertical ionization potential (IP_a/IP_v), and charge transmission (ΔN_{max}) have been computed to evaluate the reactivity of recently considered compounds, findings of all reactivity are enumerated in Table 3 besides distinctly demonstrated in Fig. 5.

$$\text{Chemical potential } (\mu) = \frac{(E_H + E_L)}{2} \quad (3)$$

The value of (μ) has been calculated using eqn (3).[58] The capacity of the electronic dispersion to discharge is described by (μ). The newly formed molecules have higher negative (−ve) chemical potential values, representing that they are extremely reactive and stable substances that are challenging to disintegrate.[58] The created molecules have a higher chemical potential value than $PC_{70}BM$, which indicates that they donate electrons more readily. Reactivity and hardness are inversely correlated, but reactivity and softness are directly correlated. The hardness and softness of the reference molecule (**AQ-R**) are 1.79 eV and 0.56 eV, respectively. However, hardness values of **AQ-1** to **AQ-8** molecules drop to 0.77, 0.88, 0.84, 0.78, 0.85, 1.54, and 0.73 eV, correspondingly, when reactivity rises while the softness values of **AQ-1** to **AQ-8** molecules rise to 1.29, 1.13, 1.19, 1.28, 1.18, 0.65, and 1.37 eV, respectively, when reactivity increases. We determined values of hardness and softness by applying eqn (4) and (5), respectively.[59,60]

$$\text{Chemical hardness } (\eta) = \frac{(E_L - E_H)}{2} \quad (4)$$

$$\text{Chemical softness } (s) = \frac{1}{\text{chemical hardness } (\eta)} \quad (5)$$

Investigating the charge transfer characteristics requires an understanding of the ionization potential (IP) and the electron affinity (EA). Molecules containing electron-donating assemblies have the least IP because they promote electron transit and destabilize the HOMO. However, molecules containing electron-deficient groups have a greater IP because electron-withdrawing groups make it difficult to remove electrons and maintain the HOMO energy level. As recommended by Koopman's theorem.[61] The IP and EA values of the entire compounds under attention were computed using eqn (6) and (7).[62] (**AQ-1**–**AQ-2**) and **AQ-R** have respective IPs of 0.21, 0.21, 0.21, 0.21, 0.21, 0.21, 0.21, 0.21, and 0.20 eV. The EAs of (**AQ-1** to **AQ-2**) and **AQ-R** are 0.11, 0.10, 0.10, 0.11, 0.10, 0.05, 0.11, and 0.02 eV, respectively.

$$\text{Ionization potential (IP)} = (E_{cation} - E_{neutral}) \quad (6)$$

$$\text{Electron affinity (EA)} = (E_{neutral} - E_{anion}) \quad (7)$$

The values of the electronegativity and electrophilicity indices, respectively, have been imitated using eqn (8) and (9).[58] Both typically have a quantitative relationship and explain why molecules take electrons. The fact that every newly developed molecule has demonstrated higher electrophilicity and electronegativity index values than the reference (**AQ-R**) supports the idea that these molecules are extremely reactive.

$$\text{Electronegativity } (\chi) = -\left(\frac{E_H + E_L}{2}\right) \quad (8)$$

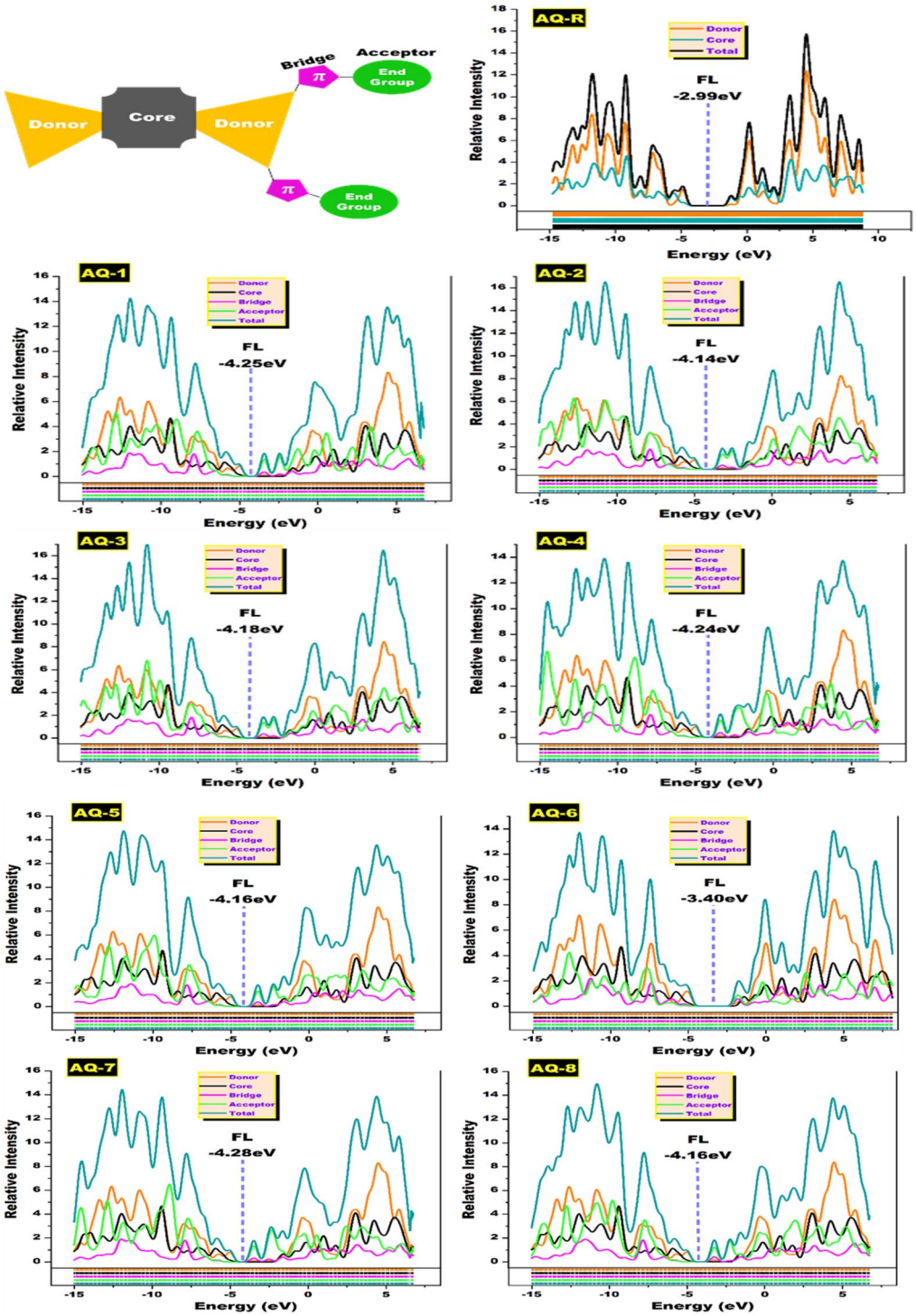

Fig. 7 Density of state analysis for synthetic reference AQ-R and designed AQ-1 to AQ-8 molecules.

$$\text{Electrophilicity index } (\omega) = \frac{\chi^2}{2(\eta)} \tag{9}$$

Another measure to examine each newly planned molecule's capacity to transfer charge is the overall extent of (ΔN_{max}), which is calculated by employing eqn (10).[63] The ability to transfer charge is higher in all freshly created molecules than in the reference (**AQ-R**). In light of the above discussion, the newly designed molecules (**AQ-1** to **AQ-8**) should be concentrated on producing superior materials for upcoming efficient solar cell devices.

Table 1 Theoretically computed outcomes of various regions in charge transfer for AQ-R and (AQ-1 to AQ-8) molecules

Molecules	Orbital	Donor (eV)	Core (eV)	Bridge (eV)	Acceptor (eV)
AQ-R	HOMO	72.5	27.5	—	—
	LUMO	14.8	85.2	—	—
AQ-1	HOMO	87.1	12.8	0.0	0.0
	LUMO	6.8	0.0	20.1	73.1
AQ-2	HOMO	86.2	13.7	0.0	0.0
	LUMO	7.0	0.0	21.3	71.7
AQ-3	HOMO	86.7	13.2	0.0	0.0
	LUMO	7.0	0.0	21.1	71.9
AQ-4	HOMO	87.2	12.7	0.0	0.0
	LUMO	7.3	0.0	21.4	71.3
AQ-5	HOMO	86.6	13.3	0.0	0.0
	LUMO	7.2	0.0	21.7	71.0
AQ-6	HOMO	81.2	18.2	0.5	0.1
	LUMO	19.8	0.0	33.9	46.3
AQ-7	HOMO	87.1	12.8	0.0	0.0
	LUMO	5.9	0.0	18.3	75.8
AQ-8	HOMO	86.7	13.2	0.0	0.0
	LUMO	8.0	0.0	23.7	68.2

$$\text{Total charge transfer } (\Delta N_{\max}) = -\frac{(\text{chemical potential})}{(\text{chemical hardness})} \quad (10)$$

3.4 Molecular electrostatic potential

The molecular electrostatic potential (MEP) is another metric that is useful in assessing the extent of electronic transmission between donor and acceptor sites. MEP directs numerous locations for the molecule related to the presence of electrons and illustrates the three-dimensional (3-D) charge dispersion that occurs in a molecule. To analyze molecular reactivity, ESP analysis was performed for compounds (**AQ-1** to **AQ-8**) under examination. By emphasizing a molecule's electrophilic and nucleophilic portions, the MEP corresponds with its reactivity. Green directs neutral areas (zero charges), blue specifies positive regions with low electron density, and red shows negative zones with high electron density on the ESP maps. The green hue of the thiophene spacers in Fig. 6 indicates that they are neutral segments of the compounds, as the red hue of the end-capped moieties specifies that they have a larger electronic density because they encompass conjugated electronegative elements, such as (O, N, and S). The suggested molecules (**AQ-1** to **AQ-8**) have considerable electronic dispersion, which is ideal for OSC devices.

3.5 Density of states analysis

To understand the electronic density, a density of states (DOS) analysis was performed at the MPW1PW91/6-31G(d,p) basis set. The DOS graph represents an increase in electron density at different energy levels. This suggests that there are a variety of potential energy levels that the electrons at this energy state can achieve. As illustrated in Fig. 7, we divided the examined molecules (**AQ-1** to **AQ-8**) into four parts, acceptor, bridge, core, and donor, which are characterized by green, pink, black, and red lines, respectively. The gray line indicates the entire DOS. The **AQ-R** fragment features red and black lines to represent the donors and core, to visualize the course of charge transition. The objective of the DOS analysis is to determine the meaningful contribution of each fragment to the compound structure with a precise number of electronic levels. It has revealed how charge is distributed from HOMO, which has a high electron-donating capacity, to LUMO, which has an electron-accepting inclination. The peak to the left of the midplane area represents the (H), and the peak to the right represents the (L).

The band distance among FMOs is essentially this core planar space. In the instance of reference **AQ-R** and created structures **AQ-1** to **AQ-8**, it was found that the end-capped units significantly improved the LUMO, spacers had a moderate influence, and the donor core had the least involvement. Table 1 displays the percentages of each fragment involved in the molecules' FMO dispersion along with the DOS plots. We determined the Fermi levels for all designed compounds (**AQ-1** to **AQ-8**), which played a role in determining the electronic density by totalling the energies of their FMOs. The **AQ-7** molecule is highly efficient among all investigated molecules due to its lower Fermi level and strong end-capped moieties, demonstrating its enhanced photovoltaic performance in optoelectronic devices as a donor molecule. It is clear from the aforementioned description that altering the terminal moieties is a useful technique for adjusting optoelectronic characteristics by closing energy gaps.

Table 2 Theoretically evaluated values of lambda max, E_x, f_{os}, and molecular orbital assignment for AQ-R and (AQ-1 to AQ-8) in DCM

Molecules	DFT calculated λ_{max} (nm)	Experimental λ_{max} (nm)	E_x (eV)	f_{os}	Major MO assignment
AQ-R	418.51	401	2.96	1.33	HOMO > LUMO (94%)
AQ-1	751.15		1.65	0.95	HOMO > LUMO (81%)
AQ-2	674.12		1.84	0.97	HOMO > LUMO (80%)
AQ-3	687.58		1.80	1.01	HOMO > LUMO (82%)
AQ-4	745.32		1.66	0.90	HOMO > LUMO (85%)
AQ-5	694.36		1.79	0.97	HOMO > LUMO (83%)
AQ-6	430.78		2.88	1.63	HOMO > LUMO (37%)
AQ-7	799.12		1.55	0.72	HOMO > LUMO (86%)
AQ-8	684.20		1.81	1.00	HOMO > LUMO (82%)

Table 3 Quantum chemical parameters including (chemical potential) μ, (hardness) η, and (softness) S, (ionization potential) IP, (electron affinity) EA, (electronegativity) χ, (electrophilicity index) ω, and (total charge transfer) ΔN_{max}, of synthetic reference **AQ-R** and designed **AQ-1**to **AQ-8** molecules

Molecules	μ (eV)	η (eV)	S (eV)	IP (eV)	EA (eV)	χ (eV)	ω (eV)	ΔN_{max} (e)
AQ-R	−2.99	1.79	0.56	0.20	0.02	2.99	2.50	1.67
AQ-1	−4.25	0.77	1.29	0.21	0.11	4.25	11.65	5.49
AQ-2	−4.14	0.88	1.13	0.21	0.10	4.14	9.71	4.69
AQ-3	−4.18	0.84	1.19	0.21	0.10	4.18	10.41	4.98
AQ-4	−4.24	0.78	1.28	0.21	0.11	4.24	11.52	5.44
AQ-5	−4.16	0.85	1.18	0.21	0.10	4.16	10.22	4.91
AQ-6	−3.40	1.54	0.65	0.21	0.05	3.40	3.75	2.20
AQ-7	−4.28	0.73	1.37	0.21	0.11	4.28	12.58	5.88
AQ-8	−4.16	0.86	1.17	0.21	0.10	4.16	10.10	4.86

3.6 Transition density matrix

The transition density matrix (TDM) study was performed using the MPW1PW91/6-31G(d,p) basis set for the entire set of recently investigated molecules (**AQ-1** to **AQ-8**). TDM investigation is crucial to understanding OSC's electronic conversions. It is possible to forecast the delocalization and coherence length of electron and hole pairs by utilizing the TDM in association with estimates about electron excitation. We divided each designed molecule into four moieties: acceptor, bridge, donor, core, and donor (A–B–D–C–D), while the reference has three fragments, excluding the acceptor and bridge fragments. To determine the localization or delocalization of the electric charge concentration at these moieties, the fragments were discriminated. Hydrogen is commonly not considered in TDM

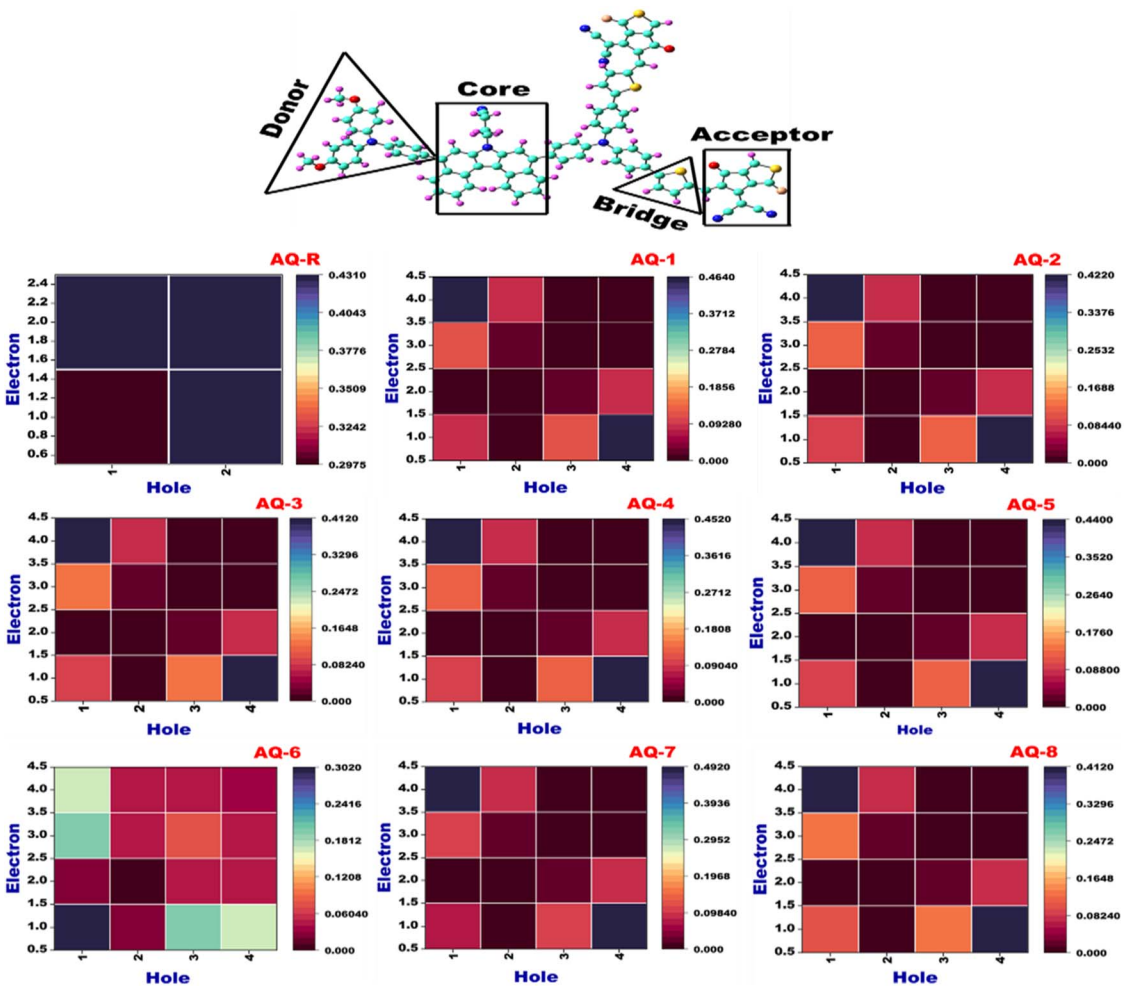

Fig. 8 Transition density matrix plots of synthetic reference **AQ-R** and designed **AQ-1** to **AQ-8** molecules.

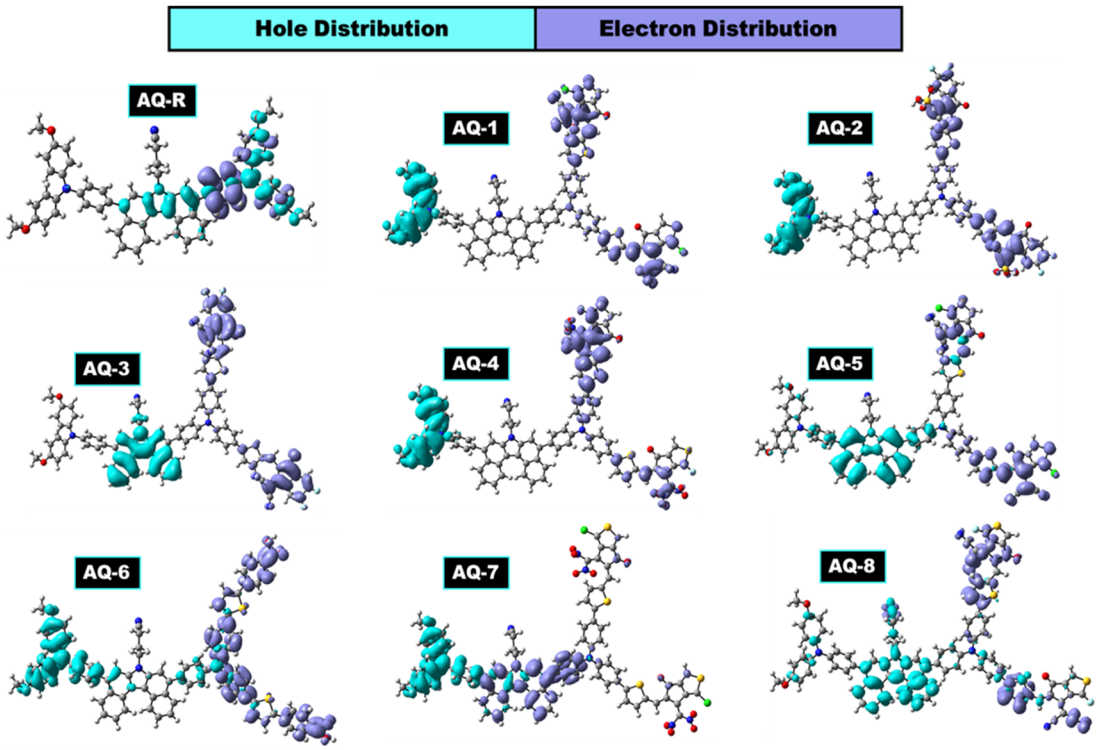

Fig. 9 Electron density difference plots of synthetic reference AQ-R and designed AQ-1 to AQ-8 molecules.

research, although it has a minimal impact on electronic transitions. TDM spectra from Fig. 8 indicated that electron consistency from the core (C) to the acceptor (A) moieties of **AQ-R** and developed molecules (**AQ-1** to **AQ-8**) is similar. These results showed that there was an equal distribution of electrical charge flexibility between the core and terminal moieties. The pattern of electronic transitions in the **AQ-R** and developed (**AQ-1** to **AQ-8**) molecules demonstrates that electron concentration has finally reached the acceptor unit. In all designed molecules, charge coherence effectively moves from the donor to the core group, then crossways to the bridge. All of the compounds were produced and demonstrated good electric transitions when compared to **AQ-R**.

3.7 Electron density difference analysis

The ICT and charge separation in all newly created donor materials were examined by computing electron density differential (EDD) schemes between S0 and S1. The blue and purple hues of the EDD plots indicate areas where electron excitation is leading to a decline in electron concentration and an intensification in it correspondingly. As can be observed in Fig. 9, the acceptor units have the highest electron densities while the donor unit has the lowest. For the modified molecules (**AQ-1** to **AQ-8**), the electron compactness over the donor is smaller than in **AQ-R**. The homogeneity of 3-D dispersal (*i.e.*, extent of delocalization) of the hole and electron, individually, was well quantified by the HDI and EDI indices. They are shown by associating hole and electron isosurface plots. The high estimated values of EDI and HDI are compatible with the localization of the electron and hole. The *t* indices also play a role in the finding value of ICT. It is clear from the positive values of the *t* indices for all newly modified (**AQ-1** to **AQ-8**) compounds that transitions from S0 to other excited levels have a large hole-to-electron separation. The Coulomb attractive

Table 4 Calculated charge transfer indices for synthetic reference AQ-R and designed (AQ-1 to AQ-8) molecules

Molecules	Dipole moment (eV)	HDI (eV)	EDI (eV)	Integral hole (amu)	Integral electron (amu)	Integral TD (amu)	*t* index (eV)	*H* index (eV)	*D* index (eV)	H_CT (eV)
AQ-R	14.81	5.40	5.62	0.824526	0.826640	0.000387	−3.43	4.642	0.159	3.590
AQ-1	1.88	8.22	4.67	1.005843	0.998703	−0.00000	21.13	6.488	24.246	3.117
AQ-2	2.22	8.07	4.62	0.988271	0.990663	0.000024	21.04	6.391	24.071	3.034
AQ-3	1.91	7.27	5.39	0.998117	0.999053	−0.00018	11.454	6.702	15.475	4.022
AQ-4	1.68	7.48	5.44	0.985234	0.985327	−0.00016	19.377	5.848	22.559	3.182
AQ-5	1.93	3.38	4.21	0.920810	0.917714	0.001063	6.879	8.541	12.584	5.706
AQ-6	11.37	5.18	4.28	0.965795	0.970665	−0.00064	7.876	8.733	14.482	6.607
AQ-7	1.70	6.00	4.26	0.923312	0.918569	−0.00296	3.675	6.155	9.009	5.335
AQ-8	1.91	6.58	3.70	0.951967	0.944098	0.000178	15.726	6.664	2.599	4.354

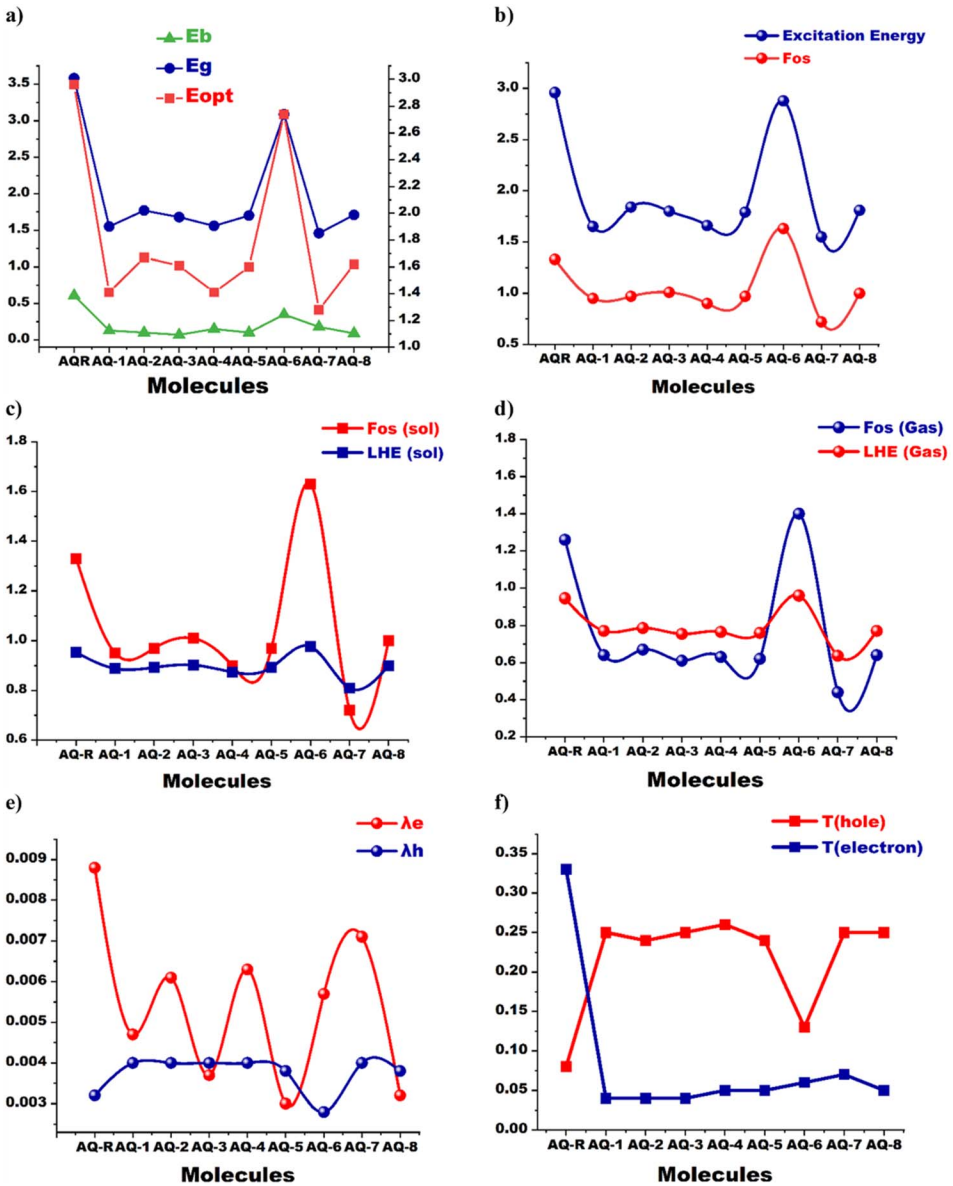

Fig. 10 (a) Comparison between E_{opt}, energy band gap, and binding energy, (b) excitation energy and oscillating intensity, (c) light harvesting efficiency and oscillator strength in dichloromethane solvent, (d) in gas medium. (e) RE plots of λ_{hole} and $\lambda_{electron}$ for **AQ-R** and (**AQ-1** to **AQ-8**) designed materials. (f) Computed values of *T*(h) and *T*(e) of model **AQ-R** besides designed molecules (**AQ-1** to **AQ-8**).

Table 5 Calculated values of (LHE) and (f_{os}) for synthetic reference, **AQ-R**, and the designed **AQ-1** to **AQ-8** molecules in DCM (solvent) and gas medium

Molecules	f_{os} (solvent)	LHE (solvent)	f_{os} (gas)	f_{os} (gas)	LHE (gas)
AQ-R	1.33	0.9532	1.26	1.26	0.9450
AQ-1	0.95	0.8878	0.64	0.64	0.7709
AQ-2	0.97	0.8928	0.67	0.67	0.7862
AQ-3	1.01	0.9023	0.61	0.61	0.7545
AQ-4	0.90	0.8741	0.63	0.63	0.7656
AQ-5	0.97	0.8928	0.62	0.62	0.7601
AQ-6	1.63	0.9766	1.40	1.40	0.9602
AQ-7	0.72	0.8095	0.44	0.44	0.6369
AQ-8	1.00	0.9000	0.64	0.64	0.7709

energy of electron–hole pairs and their electronic excitation properties are strongly correlated with the *D* index. This is the most significant determinant, as illustrated in Table 4. It is simple to hold that a greater *D* index is connected with a larger distance between the primary electron and hole distribution zones, which leads to a lower Coulomb attractive energy. According to the above findings, **AQ-1** has the lowest Coulomb attraction energy among all developed compounds because it has the maximum *D* index value. This indicates that electron-withdrawing groups lead to the transference of electronic density.

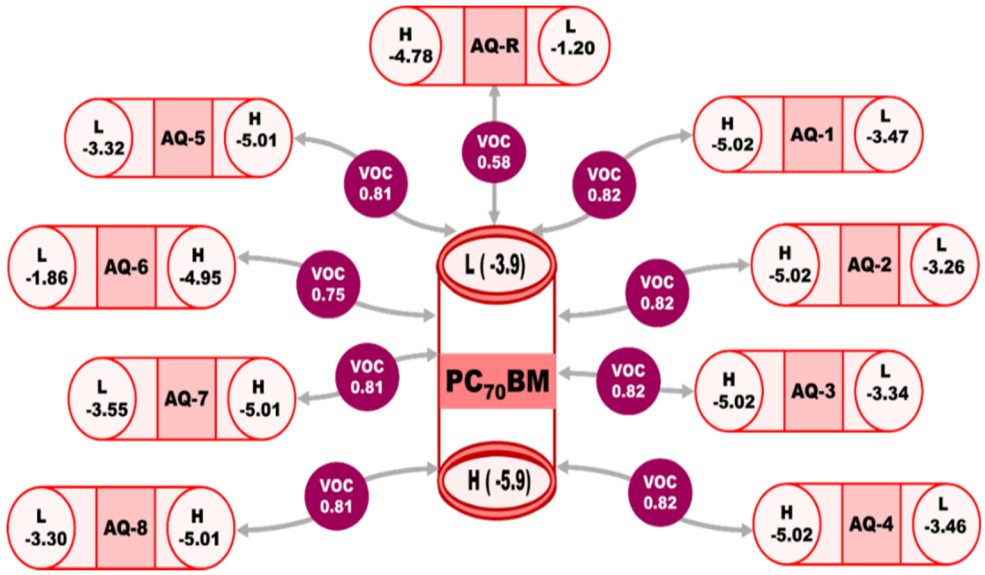

Fig. 11 The estimated open-circuit voltage values of synthetic reference AQ-R and designed AQ-1 to AQ-8 molecules, using $PC_{70}BM$ as an acceptor.

Table 6 E_{LL}, E_{CT}, energy loss, charge generation, and energy loss through charge combination for synthetic reference AQ-R and designed AQ-1 to AQ-8 molecules

Molecules	E_{LL}	E_{CT}	Energy loss during charge generation	Energy loss during charge combination
AQ-R	2.70	0.88	2.70	0.30
AQ-1	0.43	1.12	0.43	0.30
AQ-2	0.64	1.12	0.64	0.30
AQ-3	0.56	1.12	0.56	0.30
AQ-4	0.44	1.12	0.44	0.30
AQ-5	0.58	1.11	0.58	0.30
AQ-6	2.04	1.05	2.04	0.30
AQ-7	0.35	1.11	0.35	0.30
AQ-8	0.60	1.11	0.60	0.30

3.8 Heat map analysis

When assessing organic and perovskite solar cells, heat maps can be used to identify areas of the cell that are producing more heat than others. This data is also used to optimize the cell's materials and structure, increasing its efficiency. For **AQ-R** and **AQ-1** to **AQ-8**, the overlap of electrons and holes was computed theoretically. Every created molecule displays noticeable electron–hole overlaps, as seen by the plot in Fig. S2. **AQ-2** and **AQ-3** with their narrow band gaps and high electron and hole mobility. All customized molecules displayed excellent outcomes for OSC's active layer based on overlap testing.

3.9 Binding energy analysis

Another unique characteristic associated with TDMs used to assess the PV behaviour of OSCs is E_b. It is defined as the force required to differentiate the charge carriers once they have formed a connected pair. It is a significant metric for assessing the capacity of exciton detachment and the coulombic strength of the interface between electrons and holes. The E_b, calculated using eqn (11), is directly associated with coulombic interaction and, in reverse, relates to exciton dissociation.[58] Charge carriers with lower E_b can, therefore, go more easily in the direction of their appropriate electrodes. Binding energies of 0.61, 0.13, 0.10, 0.07, 0.15, 0.10, 0.35, 0.18, and 0.09 eV in (DCM) were recorded for the proposed compounds (**AQ-1** to **AQ-8**), as listed in Table S5. **AQ-3** was a molecule with remarkable optoelectronic characteristics and the lowest E_b, indicating the chief potential for charge separation, as shown in Fig. 10. Compounds with an E_b value of 0.61 eV or less are typically thought to be good PV options with encouraging V_{oc}.

$$E_b = E_g - E_{OPT} \quad (11)$$

3.10 Excitation energy analysis

Excitation energy influences electron mobility, and it is used to study the OSC's performance. Higher charge transmission is typically observed in molecules with minor E_x values. Additionally, the minimum value of excitation energy leads to a transition of electron density from donor (H) to an acceptor (L), increasing power conversion efficiency (PCE) and ultimately improving optoelectronic characteristics. The suggested molecules (**AQ-1** to **AQ-8**) had excitation energies of 1.65, 1.84, 1.80, 1.66, 1.79, 2.88, 1.55, and 1.81 eV in (DCM) and 2.02, 1.95, 2.13, 2.04, 2.84, 2.92, 1.94, and 2.87 eV in the gas phase, correspondingly. Among the designed materials, **AQ-7** displayed the highest value of λ_{max} and lowest E_x due to strong terminal moieties (nitro), indicating its exceptional potential for application in fullerene-free OSCs, as shown in Fig. 10.

3.11 Reorganization energy analysis

The proficiency of PSCs is based on the energy essential to reorganize the electrons and holes in the compound. At least

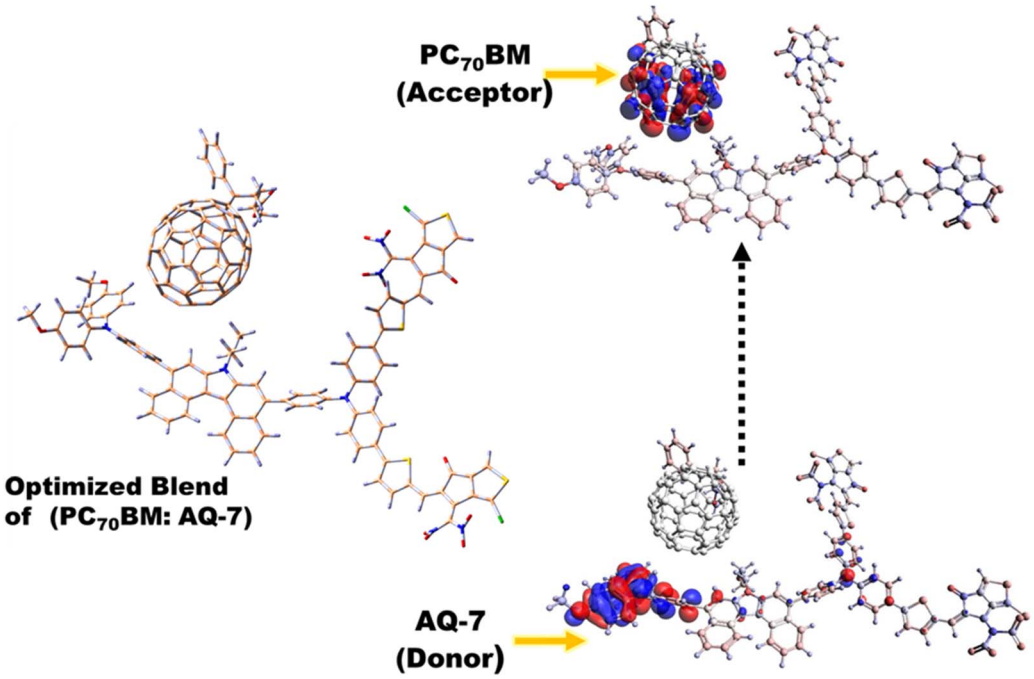

Fig. 12 Optimized blend of carbazole naphthalene-based linear HTMs **AQ-7** with polymer acceptor $PC_{70}BM$, and dispersion of H–L on **AQ-7** and $PC_{70}BM$, optimized acceptor:donor complex.

electron and hole RE, great charge movements are frequently allowed, and *vice versa*. Similar to electrons and holes, the flexibility of charges is inversely proportional to the power required to rearrange them. Therefore, a material with a small RE value is preferred for solar gadgets with maximum PCE. Two types of reorganization energy have been identified for SC compounds: internal reorganization energy (RE λ_{int}) and external reorganization energy (RE λ_{ext}). An interior reorganization might include the data associated with an unexpected alteration in interior geometric symmetry. On the other hand, one could consider atmospheric variations to be the outcome of an external restructuring force. As there are no significant alterations brought about by external influences in this instance, we will focus on the energy required for λ_{int}. In this analysis, we investigate the RE of both proposed and **AQ-R** compounds using an MPW1PW91/6-31G(d,p) basis set Fig. 10. The electron and hole reorganization energies for standard **AQ-R** and suggested materials (**AQ-1** to **AQ-8**) are displayed in Table S6. For the **AQ-R** compound, values of λ_e and λ_h are 0.0088 and 0.0032, respectively. The order in which electron mobility λ_e increases is as follows: **AQ-5** < **AQ-8** < **AQ-3** < **AQ-1** < **AQ-6** < **AQ-2** < **AQ-4** < **AQ-7** < **AQ-R**. Out of all the compounds, **AQ-5** (λ_e = 0.0030) has the lowest data of λ_e, suggesting that it has the most ability to transfer charges from contributor to acceptor moiety. The sequence of observations for hole mobility (λ_h) is as follows: **AQ-1** = **AQ-2** = **AQ-3** = **AQ-4** = **AQ-7** > **AQ-5** = **AQ-8** > **AQ-R** > **AQ-6**, suggesting that **AQ-6** has advanced hole flexibility. The RE explanation shows that the suggested compounds have operative holes and electron movement features that are compliant with **AQ-R**. The efficient photovoltaic characteristics of compounds are attributed to the terminal groups of molecules. We employed all these groups to successfully integrate functional assemblies (–SO_3H, –NO_2, F, besides CN). Fig. 10 displays the pertinent T_{hole} (transfer integral for hole) and $T_{electron}$ (transfer integral for electrons) values.

3.12 Light harvesting efficiency analysis

The capacity of a material to produce electrons during light collecting or to encourage a conducting band is similarly necessary for each constituent utilized in a PSC. The LHE was ascertained using eqn (13).[64] In this case, f stands for oscillator strength, and Table 5 displays the values of "f" that were achieved for **AQ-R** and the intended molecules (**AQ-1** to **AQ-8**).

$$J_{sc} = \int_{\lambda}^{0} \mathrm{LHE}(\lambda) \cdot \phi_{inj} \cdot \eta_{collect} \cdot d\lambda \quad (12)$$

$$\mathrm{LHE} = 1 - 10^{-f} \quad (13)$$

Furthermore, it is commonly known that this process is approximated using the following equation (eqn (12))[60] and has a direct relationship with existing data on compounds. Here, $g_{collect}$ stands for the overall charge collection, while φ_{inj} is related to the electronic injection efficiency. Importantly, both the solvent and gas phases were used for these computations, and the values used in this instance was from the solvent medium computation. Additionally, we can also practice predicted data from the gas phase for this, relying on the standard environments. In light of this, **AQ-1** (0.8878), **AQ-2** (0.8928), **AQ-3** (0.9023), **AQ-4** (0.8741), **AQ-5** (0.8928), **AQ-7** (0.8905) and **AQ-8** (0.9000) displayed lower LHE values in comparison to the **AQ-R**

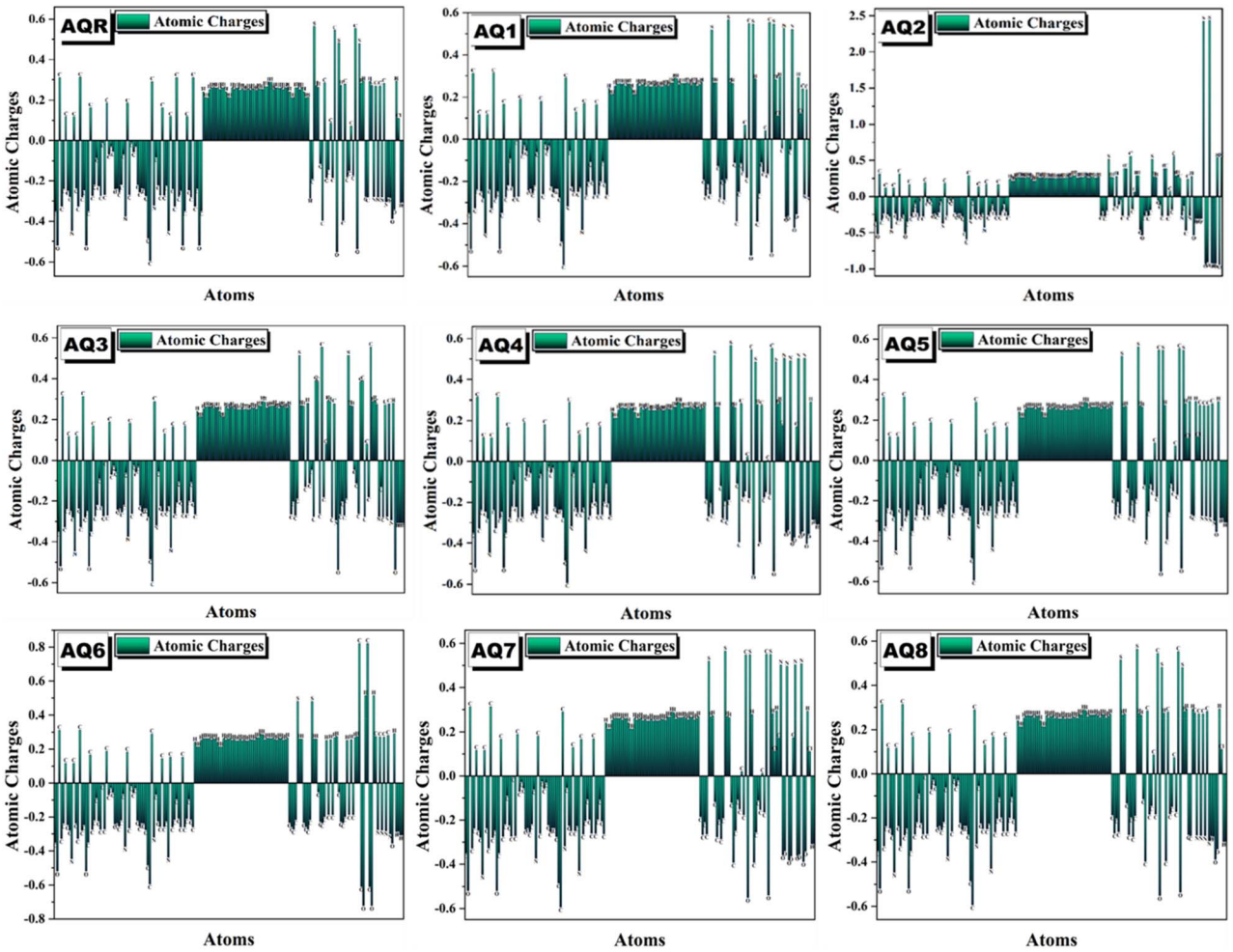

Fig. 13 Plots of the synthetic reference AQ-R and the newly created molecules AQ-1 to AQ-8 for natural population analysis.

Table 7 The quadrupole moments of synthetic reference AQ-R and freshly manufactured compounds AQ-1 to AQ-8 were calculated

Molecules	Q20 (quadrupole) values ea_{02}
AQ-R	412.2333
AQ-1	689.8883
AQ-2	723.0776
AQ-3	673.9985
AQ-4	684.6450
AQ-5	680.1997
AQ-6	557.4490
AQ-7	707.8479
AQ-8	662.7280

(0.9532); in contrast, **AQ-6** (0.9766) displays higher LHE data than **AQ-R** as illustrated in Fig. 10. Molecules with lower LHE values may have a reasonable possibility of producing higher J_{sc} values when used in the device production process. In the gas phase, the LHE and "*f*" have also been studied; relevant data are shown in Table 5.

3.13 Photovoltaic performance

The open-circuit voltage (V_{oc}) value is used to evaluate the photovoltaic capabilities and the performance of the optical device. The maximum voltage that can be produced while the circuit's current tends to zero is referred to as the V_{oc}. V_{oc} is influenced by several features, embracing the light's strength, the apparatus's optical characteristics, the energy's band gap, and others. In photovoltaic devices, the LUMO (L) of electron-withdrawing moieties is intimately connected to the HOMO (H) of certain contributor materials. The V_{oc} can be increased by enhancing the acceptor's (L) and decreasing the donor's (H). The charge shifting between the acceptor portion and donor unit was investigated using acceptor polymer PC70BM, which has an (H) value of −5.9 eV and an (L) value of −3.9 eV. These acceptors are ideally suited for the expansion of solar gadgets because their LUMO energy levels are all lower than those of donor PC70BM. The arithmetical eqn (12) (ref. 65 and 66) was practiced to determine hypothetical V_{oc} data for each of the produced configurations (**AQ-1** to **AQ-8**), along with the reference **AQ-R**.[67]

In the former equation, *e* represents the molecule's charge, which is 1, and 0.3 is a frequent value for inter-surface electron

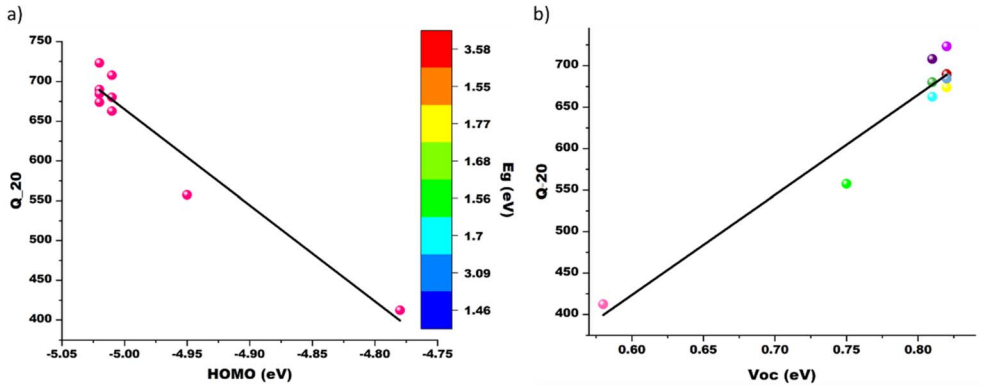

Fig. 14 (a) Quadrupole moment perpendicular to the p-system (Q20) *versus* the V_{oc} obtained for carbazole, naphthalene-based linear HTMs reference molecules, and newly synthesized chemicals. (b) The generated Q20-HOMO correlation diagram for the linear HTMs. The color of each point represents the HOMO–LUMO gap value that goes with it.

generation. The generated acceptor molecules' HOMO (H) and LUMO (L) energy levels are displayed in Fig. 11, together with the PC70BM acceptor molecule's estimated V_{oc}, as indicated in Table S7. The computed V_{oc} values for reference **AQ-R** and (**AQ-1** to **AQ-8**) were 0.58, 0.82, 0.82, 0.82, 0.82, 0.81, 0.75, 0.81, and 0.81 eV, respectively. When related to standard **AQ-R** and further synthesized complexes, tailored structures (**AQ-1** to **AQ-4**) showed the highest V_{oc}. This proved that the entire newly produced material displayed the maximum delocalization of electrons due to effective acceptor units at the terminal. In addition to the chromophores **AQ-1** to **AQ-8**, the reference **AQ-R**'s descending sequence of V_{oc} is **AQ-1** = **AQ-2** = **AQ-3** = **AQ-4** > **AQ-5** = **AQ-7** = **AQ-8** > **AQ-6** > **AQ-R.** As a result, these substances may be used to improve PCE.

$$V_{oc} = \left(\frac{E_{\text{LUMO of acceptor}} - E_{\text{HOMO of donor}}}{e} - 0.3\right) \quad (14)$$

The acceptability of intricate interfaces, or E_{LL}, has an impact on efficiency. It is the distinction between acceptor molecule's LUMO (L) and donor polymer's HOMO (H). The best E_{LL} value to inject charges from the contributor to the acceptor is between 0.2 and 1 eV, according to published studies. Additionally, we calculated the E_{LL} values for **AQ-R** and (**AQ-1** to **AQ-8**), which are shown in Table 6 and range from 0.35 to 2.70. The E_{LL} values can be calculated using eqn (15).

$$E_{LL=LD-LA} \quad (15)$$

Eqn (16) was used to calculate the interfacial charge transfer (E_{CT}) values for **AQ-R** and the recently proposed (**AQ-1** to **AQ-8**) molecules. The values vary from 0.88 to 1.12. The E_{CT} values are shown in Table 6.

$$E_{CT} = L_A - H_D \quad (16)$$

Using $E_g - E_{CT}$ and $E_{CT} - V_{oc}$, respectively, we calculated the energy loss resulting from the synthesis and combination of **AQ-R** and the newly modified (**AQ-1** to **AQ-8**) molecules. PC70BM is an excellent candidate for the donor–acceptor frontier since every molecule has a different charge generation, but the same charge loss combination.

Fill factor (FF) is another significant aspect that directly affects an OSC PCE. The donor–acceptor V_{oc} primarily determines this parameter eqn (15).[68] It is used to determine FF. In this equation, e is the reference charge, which is always 1, and V_{oc} is normalized V_{oc}. The Boltzmann constant, or k_B, is $8.61733034 \times 10-^5$ electron volts per Kelvin. T, the temperature, is a constant (300 K). The theoretical results of the normalized V_{oc} and Fill Factor (FF) are enumerated in Table S7.

$$FF = \frac{\frac{eV_{oc}}{k_B T} - \ln\left(\frac{eV_{oc}}{k_B T} + 0.72\right)}{\frac{eV_{oc}}{k_B T} + 1} \quad (17)$$

Every molecule that is generated has an FF order that corresponds to the V_{oc}. After comparison, it was determined that the freshly synthesized (**AQ-1–AQ-8**) chromophores all had higher FF as compared to the reference (**AQ-R**), with **AQ-6** having the highest FF of all. The implemented FF values for **AQ-R** and produced compounds (**AQ-1** to **AQ-8**) were 89.67, 91.07, 91.08, 91.08, 91.06, 91.04, 90.70, 91.04, and 91.04, respectively. The higher FF of the newly constructed molecules (**AQ-1** to **AQ-8**) compared to the reference means that they are more effective, and all these properties make them more beneficial in the manufacturing of OPVs.

Power conversion efficiency (PCE) is used to determine if a photovoltaic material is sufficiently efficient for practical usage by combining all of the efficient indicators of organic and perovskite solar cells into a single figure. J_{sc}, FF, and V_{oc} are all important parameters to take into account while analyzing PCE, as indicated by the provided eqn (16).[69]

$$PCE = \frac{J_{sc} V_{oc} FF}{P_{input}} \quad (18)$$

In this instance, P_{in} stands for the incident photon power on an efficient OSC; using this term would be more appropriate for these intended organic and perovskite solar cells. Herein, the external light source is denoted by P_{input}. It appears that all of the recently created compounds are superior choices for organic and perovskite solar cells, with FF and V_{oc} values that are higher than those of the reference molecule (**AQ-R**). It is well known that the J_{sc} is greatly influenced by charge flexibility rates, material band distance, in addition to LHE. We found that our proposed molecules (**AQ-1** to **AQ-8**) had a greater value than **AQ-R** Fig. S3 after performing some theoretical calculations. The PCE data of the donor materials are determined in a subsequent descending sequence: **AQ-2** > **AQ-3** > **AQ-1** > **AQ-4** > **AQ-8** > **AQ-7** > **AQ-5** > **AQ-6** > **AQ-R**. The theoretical outcomes of PCE are listed in Table S7. Thus, the development of an efficient OSCs would be more appropriate from these intended molecules.

3.14 Charge transfer analysis

An acceptor–donor complex is formed using the highly efficient designed **AQ-7** molecule and a polymer acceptor, $PC_{70}BM$, to study charge transfer. This polymer–acceptor complex study aims to examine whether a polymer acceptor, such as $PC_{70}BM$, can accept newly discovered donor material during the fabrication process. We selected this specific **AQ-7** molecule because, in addition to a strong absorption phenomenon (799.12 nm), it can show the least E_g (1.46 eV), E_x (1.55 eV), and E_b (0.18 eV). This makes it superior to the other discovered donor molecules (**AQ-1** to **AQ-6** and **AQ-8**). This polymer/donor complex unit has been optimized in single and combined states using the MPW1PW91/6-31 G(d,p) level of theory. Notably, $PC_{70}BM$ and **AQ-7** are substantially parallel to each other in the $PC_{70}BM$: **AQ-7** complex. This polymer in the donor position should aid in shifting the maximum charges to the acceptor–donor interface. We further investigated the FMOs of $PC_{70}BM$ and **AQ-7** by theoretically optimizing the blend at the MPW1PW91/6-31 G(d,p) level. Fig. 12 displays computed (H) and (L) plots of $PC_{70}BM$ and **AQ-7** molecules. In Fig. 12, the (L) level is stated over the polymer acceptor $PC_{70}BM$, while the (H) levels are altered in the donor component **AQ-7** molecule. Of these, the HOMO (H) concentration protects the area near the center; however, the (L) is dispersed on only the designed side of the molecule's bridged-core section. The results of these LUMO/HOMO dispersion pattern arrangements, which indicated that the acceptor/donor interface has the highest probability of charge transference, can be verified by looking at the formation of the charge compactness distribution that arises from two oppositely charged molecules coming parallel to one another.

3.15 Natural population analysis

The atomic charges and electron distribution of substances can be effectively ascertained using NPA. The net charges of all linear HTMs (**AQ-1** to **AQ-8**) and the reference **AQ-R** molecule, as established by natural population analysis, are shown in Fig. 13. Hydrogen has a positive charge due to its proximity to carbon, nitrogen, and sulfur atoms. All carbon atoms in the donor and acceptor are negatively charged except those bonded to the electronegative nitrogen, fluorine, sulfur, and oxygen atoms. All nitrogen atoms are negatively charged because of their connections with positively charged hydrogen and carbon atoms. As shown in **AQ-1**, **AQ-4**, and **AQ-7**, nitrogen and oxygen are connected by a positive charge. All oxygen atoms are detectable and have a negative charge, much like carbon and hydrogen. Sulfur is coupled to electronegative nitrogen and oxygen with a positive charge, and it is found in the acceptor zone and the donor part. Mulliken charge analysis indicates charge delocalization in the investigated carbazole naphthalene-based linear HTMs **AQ-R** and (**AQ-1** to **AQ-8**), which is caused by negatively charged nitrogen, oxygen, fluorine, and carbon. The abovementioned detail states that electrons are moved from the donor to the acceptor molecules. Consequently, molecules are employed as an effective material for OSC devices, and acceptor modification is a useful technique for achieving a charge separation state for the molecules being studied.

3.16 Quadrupole moment

In linear HTMs, the quadrupole moment of acceptor molecules is essential to the interfacial energetics. The HOMO–LUMO gap of a D–C–D–B–A (donor–core–donor–bridge–acceptor) kind HTM molecular architecture decreases with stronger acceptors or strong electron-withdrawing moieties. However, for the same reason, the molecule's charge flows up overall, increasing the molecular quadrupole moment. The efficient dissociation of charge transfer (CT) in carbazole naphthalene-based linear HTMs leads to gains in the internal quantum efficiency (IQE), J_{sc}, and fill factor of the solar devices. For every HTM under investigation, the quadrupole moment perpendicular to the p-system (Q20) has been computed and is displayed in Table 7. Quadrupole moments larger than **AQ-R** are seen in all computationally published carbazole naphthalene-based linear HTMs, suggesting strong OSC potential and substantial J_{sc}. As illustrated in Fig. 14, the calculated Q20 values were also compared with the highest and lowest occupied molecular orbital (HOMO and LUMO) of each molecule. Fig. 14 clearly shows that a bigger HOMO–LUMO gap produces a smaller Q20. These donor molecules have a narrow HOMO–LUMO gap of less than 3 eV with Q20 values ranging from 412 to 723 ea_{02}. The observed trend suggests that carbazole naphthalene-based linear HTMs with narrow HOMO–LUMO gap (1.77 eV) and a Q20 value of 723 ea_{02} could be a good acceptor. It is used for bulk heterojunction OSC, despite the short sample size. Additionally, these acceptors have the biggest λ_{max} in the near-infrared spectrum, which may improve the visible range absorption of donor photons and produce a mixture effective at photon harvesting.

4 Conclusions

In this study, eight novel donor molecules (**AQ-1** to **AQ-8**) featuring a D–C–D–B–A framework were theoretically designed by modifying the terminal donor groups of the reference molecule (**AQ-R**) with various electron-accepting units to improve the performance of solar cell devices. These structural

modifications significantly lowered the energy band gaps of the new molecules, with values ranging from 1.46 to 3.09 eV, markedly reduced compared to **AQ-R** (3.58 eV). Notably, the experimental λ_{max} of **AQ-R** (401 nm) closely matched the DFT-predicted value of 418.51 nm, confirming the reliability of the theoretical approach. The newly designed molecules displayed extended absorption bands with pronounced bathochromic shifts, indicating improved light-harvesting capabilities. In the gas phase, their absorption maxima spanned 424.65–638.07 nm, while in DCM solvent, they extended further to 430.78–799.12 nm, considerably broader than those of **AQ-R**. The minimal transition energies observed (as low as 408.76 nm in gas and 418.51 nm in DCM) further support their enhanced optoelectronic behavior. The DOS plots revealed that all the developed compounds have lower Fermi levels and strong end-capped moieties, demonstrating their enhanced photovoltaic performance in optoelectronic devices as a donor molecule. TDM spectra demonstrate that electronic concentration has finally reached the acceptor unit, and in all designed molecules (**AQ-1** to **AQ-8**), charge coherence effectively moves from the donor to the core group, then crossways to the bridge. In MEP plots, several charging sites demonstrate unique properties of the molecules that can boost the PCE of solar cells. The designed molecules (**AQ-1** to **AQ-8**) and reference *R* exhibit almost identical charging sites, indicating the success of our end-capped engineering for the practical synthesis of OSCs and PSCs.

Reorganization energies (RE) for both electrons and holes were favorably low in the designed molecules, ranging from 0.0030–0.0071 eV and 0.0028–0.0040 eV, respectively, an improvement over **AQ-R**'s electron RE of 0.0088 eV. Among all candidates, **AQ-2** exhibited the highest open-circuit voltage (0.82 eV), fill factor (91.08%), and PCE value of 18.08%, highlighting its strong potential for high-performance solar applications. Charge transfer analysis of the **AQ-7**:$PC_{70}BM$ complex demonstrated efficient electron migration from the HOMO to the LUMO, confirming its aptitude for effective charge separation. Furthermore, MEP, density of states, TDM, electron density difference, and hole–electron overlap analyses provided deeper insight into the charge distribution and interaction mechanisms within these materials. Overall, the findings strongly suggest that these newly developed donor compounds are promising candidates for incorporation into next-generation organic and perovskite photovoltaic devices.

Author contributions

AG: writing – original draft, conceptualization, methodology, data curation, formal analysis. ZI: conceptualization, supervision, validation, methodology, formal analysis, writing-review, and editing. RH: methodology, project administration, supervision, formal analysis, visualization, data curation, validation, resources, writing – review, and editing. AG: data curation, investigation, visualization, riting – review, and editing. HWD: software, resources, data curation, funding acquisition, writing – review editing. MMAI: conceptualization, formal analysis, data curation, writing – review editing. MA: conceptualization, methodology, data curation, project administration, supervision, writing – review and editing.

Conflicts of interest

The author declares that they have no competing interests.

Data availability

All data associated with this article are provided in the SI. Supplementary information: Geometrical optimized structures of reference and designed molecules, heat map plots, theoretical and experimentally determined optical properties, computed values of energy gap, excitation energy, and oscillating strength, arithmetically measured values of dihedral angles, calculated values of binding and reorganization energy, and all materials' photovoltaic characteristics. See DOI: **https://doi.org/10.1039/d5ra06095h**.

Acknowledgements

The authors thank COMSAT University Islamabad, Abbotabad Campus for providing their state-of-the-art computational facilities. The authors extend their appreciation to the Ongoing Research Funding Program (ORF-2025-812), King Saud University, Riyadh, Saudi Arabia, for funding this work.

References

1 M. Panneerselvam, A. Kathiravan, R. V. Solomon and M. Jaccob, *Phys. Chem. Chem. Phys.*, 2017, **19**, 6153–6163.
2 A. M. Makarieva, V. G. Gorshkov and B.-L. Li, *Ecol. Complex.*, 2008, **5**, 281–288.
3 R. Avtar, N. Sahu, A. K. Aggarwal, S. Chakraborty, A. Kharrazi, A. P. Yunus, J. Dou and T. A. Kurniawan, *Resources*, 2019, **8**, 149.
4 M. Salim, M. Rafiq, R. A. Khera, M. Arshad and J. Iqbal, *Sol. Energy*, 2022, **233**, 31–45.
5 M. Khalid, I. Shafiq, M. Zhu, M. U. Khan, Z. Shafiq, J. Iqbal, M. M. Alam, A. A. C. Braga and M. Imran, *J. Saudi Chem. Soc.*, 2021, **25**, 101305.
6 A. Polman, M. Knight, E. C. Garnett, B. Ehrler and W. C. Sinke, *Science*, 2016, **352**, aad4424.
7 H. Hardianto, *Int. J. Environ. Eng. Educ.*, 2019, **1**, 1–8.
8 Z. Afzal, R. Hussain, M. U. Khan, M. Khalid, J. Iqbal, M. U. Alvi, M. Adnan, M. Ahmed, M. Y. Mehboob and M. Hussain, *J. Mol. Model.*, 2020, **26**, 137.
9 A. Kojima, K. Teshima, Y. Shirai and T. Miyasaka, *J. Am. Chem. Soc.*, 2009, **131**, 6050–6051.
10 Y. Zhao, F. Ma, Z. Qu, S. Yu, T. Shen, H.-X. Deng, X. Chu, X. Peng, Y. Yuan and X. Zhang, *Science*, 2022, **377**, 531–534.
11 J. Park, J. Kim, H.-S. Yun, M. J. Paik, E. Noh, H. J. Mun, M. G. Kim, T. J. Shin and S. I. Seok, *Nature*, 2023, **616**, 724–730.
12 S. Sahare, H. D. Pham, D. Angmo, P. Ghoderao, J. MacLeod, S. B. Khan, S. L. Lee, S. P. Singh and P. Sonar, *Adv. Energy Mater.*, 2021, **11**, 2101085.

13 G. Saianand, P. Sonar, G. J. Wilson, A.-I. Gopalan, V. A. Roy, G. E. Unni, K. M. Reza, B. Bahrami, K. Venkatramanan and Q. Qiao, *J. Energy Chem.*, 2021, **54**, 151–173.
14 National Renewable Energy Laboratory, *Best Research-Cell Efficiency Chart*, **https://www.nrel.gov/pv/cell-efficiency.html**, accessed September 2025.
15 C. Huang, W. Fu, C.-Z. Li, Z. Zhang, W. Qiu, M. Shi, P. Heremans, A. K.-Y. Jen and H. Chen, *J. Am. Chem. Soc.*, 2016, **138**, 2528–2531.
16 S. Paek, P. Qin, Y. Lee, K. T. Cho, P. Gao, G. Grancini, E. Oveisi, P. Gratia, K. Rakstys and S. A. Al-Muhtaseb, *Adv. Mater.*, 2017, **29**, 1606555.
17 H. D. Pham, T. T. Do, J. Kim, C. Charbonneau, S. Manzhos, K. Feron, W. C. Tsoi, J. R. Durrant, S. M. Jain and P. Sonar, *Adv. Energy Mater.*, 2018, **8**, 1703007.
18 H. D. Pham, S. M. Jain, M. Li, Z. K. Wang, S. Manzhos, K. Feron, S. Pitchaimuthu, Z. Liu, N. Motta and J. R. Durrant, *Adv. Electron. Mater.*, 2020, **6**, 1900884.
19 H. D. Pham, S. M. Jain, M. Li, S. Manzhos, K. Feron, S. Pitchaimuthu, Z. Liu, N. Motta, H. Wang and J. R. Durrant, *J. Mater. Chem. A*, 2019, **7**, 5315–5323.
20 K. Kranthiraja, H. Kwon, Y.-S. Gal, J. W. Lee and S.-H. Jin, *Mol. Cryst. Liq. Cryst.*, 2018, **660**, 54–59.
21 H. D. Pham, H. Hu, K. Feron, S. Manzhos, H. Wang, Y. M. Lam and P. Sonar, *Sol. RRL*, 2017, **1**, 1700105.
22 K. Rakstys, C. Igci and M. K. Nazeeruddin, *Chem. Sci.*, 2019, **10**, 6748–6769.
23 X. Liu, K. Wang, R. Liu, L. Yan, P. Dong, H. Zhao, Z. Wang, Y. Wu, P. Yin and K. Guo, *Dyes Pigm.*, 2022, **204**, 110452.
24 J. Chen, R. Ghadari, X. Zhang, M. Han, X. Liu, Y. Zhou, J. Chen, B. Li, H. Quan, Y. Ding, M. Cai and S. Dai, *Dyes Pigm.*, 2024, **222**, 111913.
25 Y. Wang, L. Duan, M. Zhang, Z. Hameiri, X. Liu, Y. Bai and X. Hao, *Sol. RRL*, 2022, **6**, 2200234.
26 E. Rezaee, X. Liu, Q. Hu, L. Dong, Q. Chen, J.-H. Pan and Z.-X. Xu, *Sol. RRL*, 2018, **2**, 1800200.
27 X. Yin, Z. Song, Z. Li and W. Tang, *Energy Environ. Sci.*, 2020, **13**, 4057–4086.
28 B. Xu, E. Sheibani, P. Liu, J. Zhang, H. Tian, N. Vlachopoulos, G. Boschloo, L. Kloo, A. Hagfeldt and L. Sun, *Adv. Mater.*, 2014, **26**, 6629–6634.
29 P. Zhang, K. Chen, X. Gao, J. Zhang, Y. Zeng, R. Tang, F. Wu, C. Zhong and L. Zhu, *Dyes Pigm.*, 2023, **220**, 111693.
30 X. Liu, B. Ding, M. Han, Z. Yang, J. Chen, P. Shi, X. Xue, R. Ghadari, X. Zhang and R. Wang, *Angew. Chem.*, 2023, **135**, e202304350.
31 Y. Liu, F. Liu, J. Wang, H. Huang, S. Yan, S. Gao, L. Wang, W. Huang and T. Qin, *Dyes Pigm.*, 2021, **188**, 109164.
32 H. Choi, S. Paek, N. Lim, Y. H. Lee, M. K. Nazeeruddin and J. Ko, *Chem. - Eur. J.*, 2014, **20**, 10894–10899.
33 J. Wang, Y. Chen, M. Liang, G. Ge, R. Zhou, Z. Sun and S. Xue, *Dyes Pigm.*, 2016, **125**, 399–406.
34 A. Krishna, D. Sabba, H. Li, J. Yin, P. P. Boix, C. Soci, S. G. Mhaisalkar and A. C. Grimsdale, *Chem. Sci.*, 2014, **5**, 2702–2709.
35 Z. Shariatinia, *Sol. Energy*, 2022, **236**, 548–560.
36 H. D. Pham, T. C.-J. Yang, S. M. Jain, G. J. Wilson and P. Sonar, *Adv. Energy Mater.*, 2020, **10**, 1903326.
37 H. M. Diab, A. M. Abdelmoniem, M. R. Shaaban, I. A. Abdelhamid and A. H. M. Elwahy, *RSC Adv.*, 2019, **9**, 16606–16682.
38 P. G. Kadam and S. Mhaske, *Des. Monomers Polym.*, 2011, **14**, 515–540.
39 K. Rakstys, S. Paek, A. Drevilkauskaite, H. Kanda, S. Daskeviciute, N. Shibayama, M. Daskeviciene, A. Gruodis, E. Kamarauskas, V. Jankauskas, V. Getautis and M. K. Nazeeruddin, *ACS Appl. Mater. Interfaces*, 2020, **12**, 19710–19717.
40 F. Abbas, M. D. Mohammadi, H. Louis, I. O. Amodu, D. E. Charlie and T. E. Gber, *Mater. Sci. Eng., B*, 2023, **291**, 116392.
41 H. Louis, T. O. Unimuke, J. O. Ikenyirimba, G. E. Mathias and A. S. Adeyinka, *Chem. Afr.*, 2023, **6**, 2665–2675.
42 F. Abbas, M. D. Mohammadi, H. Louis and E. C. Agwamba, *J. Mol. Model.*, 2023, **29**, 31.
43 G. J. Ogunwale, H. Louis, I. O. Amodu, D. E. Charlie, I. J. Ikot, P. O. Olagoke and A. S. Adeyinka, *Comput. Theor. Chem.*, 2023, **1220**, 114003.
44 E. C. Agwamba, H. Louis, T. O. Unimuke, U. S. Ameuru, G. E. Mathias, U. G. Chukwu, L. Obojor-Ogar, U. J. Undiandeye and E. A. Eno, *J. Indian Chem. Soc.*, 2022, **99**, 100739.
45 H. Louis, E. A. Eno, R. A. Timothy, E. C. Agwamba, T. O. Unimuke, P. T. Bukie, I. E. Chukwudubem and O. E. Offiong, *Opt. Quantum Electron.*, 2022, **54**, 681.
46 M. Frisch, G. Trucks, H. Schlegel, G. Scuseria, M. Robb, J. Cheeseman, J. Montgomery JrT. Vreven, K. Kudin and J. Burant, *Gaussian 03, Revision C.02*, Gaussian Inc., Wallingford, CT, 2004.
47 R. Dennington, T. A. Keith and J. M. Millam, *GaussView 6.0*, Gaussian Inc., Wallingford, 2008, p. 20.
48 B. Civalleri, C. M. Zicovich-Wilson, L. Valenzano and P. Ugliengo, *CrystEngComm*, 2008, **10**, 405–410.
49 T. Yanai, D. P. Tew and N. C. Handy, *Chem. Phys. Lett.*, 2004, **393**, 51–57.
50 Y. Zhao and D. G. Truhlar, *Theor. Chem. Acc.*, 2008, **120**, 215–241.
51 S. A. Siddique, M. Arshad, S. Naveed, M. Y. Mehboob, M. Adnan, R. Hussain, B. Ali, M. B. A. Siddique and X. Liu, *RSC Adv.*, 2021, **11**, 27570–27582.
52 C. Adamo and V. Barone, *J. Chem. Phys.*, 1998, **108**, 664–675.
53 J.-D. Chai and M. Head-Gordon, *Phys. Chem. Chem. Phys.*, 2008, **10**, 6615–6620.
54 V. Barone and M. Cossi, *J. Phys. Chem. A*, 1998, **102**, 1995–2001.
55 N. M. O'boyle, A. L. Tenderholt and K. M. Langner, *J. Comput. Chem.*, 2008, **29**, 839–845.
56 T. Lu and F. Chen, *J. Comput. Chem.*, 2012, **33**, 580–592.
57 R. A. Marcus, *Pure Appl. Chem.*, 1997, **69**, 13–30.
58 A. S. Rad and K. Ayub, *Mater. Res. Bull.*, 2018, **97**, 399–404.
59 A. Martínez, I. Membrillo, V. M. Ugalde-Saldívar and L. Gasque, *J. Phys. Chem. B*, 2012, **116**, 8038–8044.

60 J. L. Gázquez, A. Cedillo and A. Vela, *J. Phys. Chem. A*, 2007, **111**, 1966–1970.
61 C.-G. Zhan, J. A. Nichols and D. A. Dixon, *J. Phys. Chem. A*, 2003, **107**, 4184–4195.
62 Y. Li, C. Sun, P. Song, F. Ma and Y. Yang, *ChemPhysChem*, 2017, **18**, 366–383.
63 J. Padmanabhan, R. Parthasarathi, V. Subramanian and P. K. Chattaraj, *J. Phys. Chem. A*, 2007, **111**, 1358–1361.
64 A. Ostovan, Z. Mahdavifar and M. Bamdad, *Polymer*, 2017, **126**, 162–176.
65 N. K. Elumalai and A. Uddin, *Energy Environ. Sci.*, 2016, **9**, 391–410.
66 S. J. Akram, J. Iqbal, M. Ans, Y. A. El-Badry, R. F. Mehmood and R. A. Khera, *Sol. Energy*, 2022, **237**, 108–121.
67 M. C. Scharber, D. Mühlbacher, M. Koppe, P. Denk, C. Waldauf, A. J. Heeger and C. J. Brabec, *Adv. Mater.*, 2006, **18**, 789–794.
68 Qundeel, M. Adnan, R. Hussain, R. A. Shehzad, S. Muhammad, G. Mustafa and Z. Irshad, *Int. J. Quantum Chem.*, 2024, **124**, e27344.
69 A. Rasool, S. Zahid, M. Ans, J. Iqbal, M. Adnan, E.-S. M. Sherif and M. S. Al-Buriahi, *Opt. Mater.*, 2022, **123**, 111907.